

## Islands in Zonal Flow\*

MICHAEL A. SPALL

*Department of Physical Oceanography, Woods Hole Oceanographic Institution, Woods Hole, Massachusetts*

(Manuscript received 1 April 2003, in final form 9 June 2003)

### ABSTRACT

The impact of a meridional gradient in sea surface temperature (warm toward the equator, cold toward the pole) on the circulation around an island is investigated. The upper-ocean eastward geostrophic flow that balances such a meridional gradient is blocked where the isotherms intersect boundaries. In the case in which the boundaries represent either the eastern or western side of a planetary-scale island, circulation integrals around the island show that some of this eastward transport will flow around both the equatorward and poleward tips of the island. There is also a net downwelling along the western side of the island and a net upwelling along the eastern side of the island. An analytic model of the eastern and western boundary currents is used together with a circulation integral to estimate the fraction of the eastward transport that flows around the equatorward and poleward tips of the island and the net upwelling/downwelling on either side of the island. Calculations with a primitive equation numerical model are in close agreement with the theory. A simple closed-form analytic solution for the transport around the island tips is derived in the limit of strong buoyancy forcing. It is found that, over a wide range of parameter space, a significant fraction of the eastward transport in the upper ocean circulates around the tips of the island from the western basin into the eastern basin.

### 1. Introduction

Theoretical understanding of what drives the circulation around planetary-scale islands is based largely on circulation integrals of the wind-driven momentum equation. Godfrey (1989) derived a simple and powerful relationship between the net wind stress curl to the east of an island and the depth integrated circulation around the island, which has come to be called the island rule. The advantage of this approach is that the circulation integral avoids the eastern boundary of the island, where dissipation is likely to be important, and requires only knowledge of the large-scale wind field and geometry of the island. In its most simple form, the island rule neglects time dependence; nonlinearity; dissipation along the northern, southern, and western sides of the island; baroclinicity; and bottom topography. Godfrey and Masumoto (1999) diagnosed the balance of terms along an integration path that encircles Australia in a general circulation model and found that some terms not considered in the original island rule were not small (such as pressure drop along south Australia, upwelling,

and the pressure drop across New Zealand) but they tended to cancel each other so that the original island rule gave a reasonably good estimate of the total depth integrated throughflow in the model. Wajoswicz (1993) and Pratt and Pedlosky (1998) have extended the island rule to consider dissipation along the northern, southern, and western boundaries as a result of wind-forced circulations. Time dependence has also been considered by Wajoswicz (1995), Pedlosky and Spall (1999), and Firing et al. (1999).

The island rule has been commonly applied to estimate the depth-integrated strength of the Indonesian Throughflow (e.g., Godfrey 1989, 1996; Wajoswicz 1993). However, estimates of the vertical distribution of the Indonesian Throughflow suggest that the transport from the Pacific Ocean into the Indian Ocean has a subsurface maximum somewhere between 100-m and 300-m depth. Dynamic height differences between Australia and Java along a section in the eastern Indian Ocean indicate a maximum throughflow strength near 150-m depth (Godfrey 1989). Recent current-meter and acoustic Doppler profiler measurements in the Makassar Strait, which is believed to carry most of the throughflow transport, also suggest a subsurface maximum near 200–250 m (Gordon et al. 1999). Temperature, salinity, and passive tracers in the source regions of the throughflow are strong functions of depth (Gordon 1986; Field et al. 2000), and so the baroclinic structure of the throughflow is important in determining the net flux of these properties between the Pacific and Indian Oceans.

---

\* Woods Hole Oceanographic Institution Contribution Number 10389.

---

Corresponding author address: Dr. Michael A. Spall, MS 21, 360 Woods Hole Road, Woods Hole Oceanographic Institution, Woods Hole, MA 02543.  
E-mail: mspall@whoi.edu

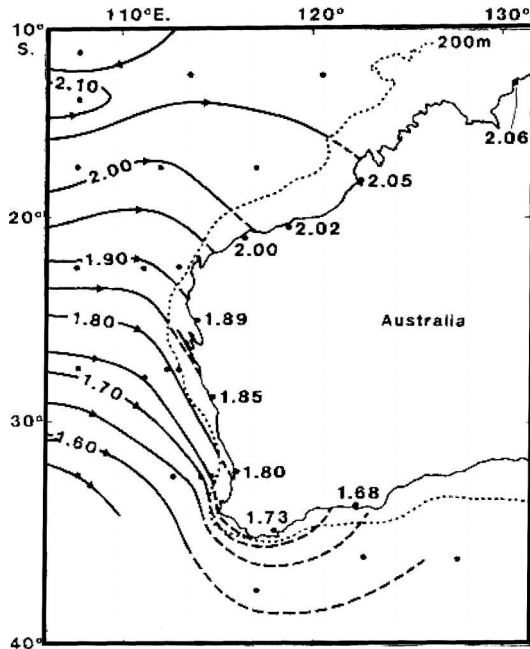


FIG. 1. Sea surface dynamic height (m) referenced to 1300 m, from Godfrey and Ridgway (1985).

Buoyancy forcing has generally been neglected in theories of the circulation around planetary-scale islands. For large islands in midlatitudes, the sea surface density at the poleward tip of the island can be much greater than that at the equatorward tip of the island. For example, the land masses and shallow seas of Australia and New Guinea extend from near the equator to approximately 44°S. The sea surface temperature at the poleward tip of Australia is approximately 15°C cooler than it is at the equator. Similar meridional gradients of sea surface temperature are found along other planetary-scale islands such as New Zealand, Madagascar, Hawaii, and Japan.

In general, the decrease in sea surface temperature with increasing latitude will drive a geostrophically balanced eastward upper-ocean flow. For example, the upper-ocean steric height gradient in the interior of the Indian Ocean drives a surface-intensified eastward flow toward the west coast of Australia (Fig. 1, from Godfrey and Ridgway 1985). As the flow approaches the boundary, dissipation becomes important, steric height contours intersect the boundary, and the current flows down the pressure gradient toward the pole in the form of a narrow boundary current called the Leeuwin Current. This warm water is subsequently cooled by heat loss to the atmosphere, resulting in strong turbulent mixing and deep mixed layers. A similar equatorward eastern boundary current is forced at depths below the Leeuwin Current. There is a similar change in steric height along the east coast of Australia, but the effects of this gradient on the boundary current structure are more difficult to discern because of the dominance of the wind-driven

western boundary current. Such buoyancy-forced changes in pressure along the boundaries of an island have not yet been considered in wind-driven-only theories.

The purpose of the present study is to characterize the buoyancy-forced circulation around an island in the presence of a meridional gradient in sea surface temperature. Although the general problem is motivated by islands such as Australia and New Zealand, the approach is quite idealized and designed to gain a general understanding of the circulation near the boundaries of the island, the net exchange between basins to the east and west of the island, and how these quantities depend on the island size and strength of buoyancy forcing.

## 2. A simple model of buoyancy-forced boundary currents

A simple, analytic model of buoyancy-forced boundary currents is now developed in order to demonstrate and quantify how a meridional gradient in sea surface temperature influences the baroclinic circulation around large islands. This approach has some elements in common with previous models of buoyancy-forced boundary currents, such as those of the Leeuwin Current (e.g., McCreary et al. 1986; Thompson 1987; Weaver and Middleton 1990; Godfrey and Weaver 1991) and the general two-level model of Davey (1983). While the details of these models differ, they include two essential features. Each model has a meridional pressure (or temperature) gradient in the ocean interior. Each of the models also has a means to trap Rossby waves near an eastern boundary, as is required to maintain an eastern boundary current in the face of westward Rossby wave propagation. The trapping is achieved in the model of McCreary et al. (1986) by vertical diffusion of density, which is imposed at the surface, while the models of Thompson (1987) and Weaver and Middleton (1990) trap waves by including a sloping bottom near the eastern boundary. The model of Davey (1983) restores the upper-ocean temperature toward an atmospheric temperature with a specified timescale. Nonlinearities resulting from interactions between vertical modes may also be important in maintaining eastern boundary currents, as discussed by McCreary et al. (1992). The model developed here is most similar to the two-level model of Davey (1983). It maintains a meridional pressure gradient and arrests the westward propagation of Rossby waves by parameterizing heat exchange with the atmosphere. The relatively simple nondimensional formulation allows for analytic and, in some cases, closed-form solutions. These solutions provide some new insights into the structure of buoyancy-forced eastern and western boundary currents, particularly on planetary scales. However, the most important distinction of this analysis is that the circulation takes place around an island.

The model solves for the steady circulation in a plan-

etary geostrophic fluid subject to buoyancy forcing. The planetary geostrophic approximation is important for large-scale motions because it retains the dependence of the planetary Rossby wave phase speed on latitude and the horizontal divergences arising from the meridional variation in the Coriolis parameter. The starting point is the linear vorticity equation with lateral viscosity,

$$\beta^*v = fw_z + A_h \nabla^2 \zeta, \quad (1)$$

where  $f = f_0 + \beta^*y$  is the Coriolis parameter;  $w$  is the vertical velocity;  $A_h$  is the lateral viscosity coefficient;  $\zeta = v_x - u_y$  is the relative vorticity;  $v, u$  are the meridional and zonal velocities; and subscripts indicate partial differentiation. The analytic model consists of a single moving layer of thickness  $h$  and a deep, motionless ocean.

The model is forced by restoring the layer thickness  $h$  toward a specified thickness  $\mathcal{H}(y)$  with timescale  $\gamma$ . This variation in thickness (or pressure) of the layer with latitude is the layer-model equivalent of a meridional density gradient. Restoring the model thickness toward a thickness that decreases poleward is a parameterization of buoyancy forcing by heat exchange with an atmosphere that is warm near the equator and cool toward the Pole. When the moving layer is thicker than  $\mathcal{H}$ , the layer thickness is reduced by transferring mass into the deep ocean. Because the lower layer is of higher density, this flux corresponds to heat loss to the atmosphere, cooling, and downwelling. This mass exchange may be expressed in terms of the vertical velocity at the layer interface as

$$w = \frac{\mathcal{H} - h}{\gamma} = \frac{-P}{\gamma g'}, \quad (2)$$

where the integrated hydrostatic relation  $p = g'h$  has been used and  $g'$  is the reduced gravity between the upper layer and the deep ocean. The total pressure  $p = \mathcal{P} + P$  has been decomposed into a large-scale component that varies only in the meridional direction,  $\mathcal{P} = g'\mathcal{H}$ , and a perturbation  $P$  that arises as a result of the meridional boundary.

It is assumed that the meridional velocity is in geostrophic balance and that the deep flow is motionless so that  $v = p_x/f$ . Anticipating narrow meridional eastern and western boundary currents, it is further assumed that  $v_x \gg u_y$  and  $P_{xyy} \ll P_{xxx}$ . The coordinate  $x = 0$  on the boundary,  $x < 0$  for eastern boundary current solutions, and  $x > 0$  for western boundary current solutions. The linear vorticity equation may now be written in terms of the perturbation pressure as

$$\beta^*P_x = \frac{f^2 P}{g'H\gamma} + A_h P_{xxx}, \quad (3)$$

where the mean thickness of the layer is  $H$ . It is useful to nondimensionalize the vorticity equation with the following scaling:

$$P \propto \frac{V\delta}{f_0}, \quad x, y \propto \delta, \quad v, u \propto V, \quad \text{and} \\ f = f_0 \left( 1 + \frac{\beta^* \delta y}{f_0} \right). \quad (4)$$

The nondimensional latitude  $y$  is now referenced to a central latitude  $y_0$  and  $\delta$  is the viscous boundary layer width (defined below). Substitution into (3) results in a nondimensional equation for the perturbation pressure  $P$ :

$$P_{xxxx} - P_x + (1 + \beta y)^2 \left( \frac{\delta}{\delta_T} \right) P = 0. \quad (5)$$

There are two important length scales in the problem. The first is the viscous boundary layer width  $\delta = (A_h/\beta^*)^{1/3}$ , which is the same length scale that arises in the classical wind-driven western boundary layer theory (Munk 1950). The second length scale,  $\delta_T = \beta^*g'H\gamma/f_0^2$ , is the distance a baroclinic Rossby wave propagates over the damping timescale  $\gamma$  (e.g., Davey 1983; Kawase 1987). The nondimensional  $\beta = \beta^*\delta/f_0$  is a measure of the variation of the Coriolis parameter over the viscous length scale  $\delta$ .

The solution to (5) is obtained by assuming the form

$$P(x, y) = A(y)e^{ikx}. \quad (6)$$

Substitution of (6) into (5) results in an equation for the roots  $k$ :

$$k^4 - ik + (1 + \beta y)^2 \left( \frac{\delta}{\delta_T} \right) = 0. \quad (7)$$

The dependence of the roots on latitude  $y$  arises because the Rossby wave phase speed decreases as  $f^{-2}$  for planetary geostrophic dynamics. Two of the roots of (7) have negative imaginary components ( $k_1, k_2$ ) and two of the roots have positive imaginary components ( $k_3, k_4$ ). Roots  $k_1, k_2$  provide bounded solutions of the form (6) for eastern boundary currents and roots  $k_3, k_4$  provide bounded solutions for western boundary currents.

The imaginary parts of  $k_1$  and  $k_2$  are given by the solid lines in Fig. 2 as a function of  $\delta/\delta_T$  ( $y$  is taken to be zero here). The imaginary part of the roots controls the exponential decay of the boundary layer structure with distance offshore. For  $\delta/\delta_T < 0.48$  (very weak buoyancy forcing) there are two distinct negative imaginary components. As  $\delta/\delta_T \rightarrow 0$ , solution of (7) shows that one imaginary component approaches  $-i(1 - \delta/\delta_T)$  and the other approaches  $-i\delta/\delta_T$ . The larger of these two branches corresponds to a dimensional offshore decay scale of  $\delta$  (the standard viscous eastern boundary layer of wind-driven theory) while the smaller branch corresponds to a dimensional offshore decay scale of  $\delta_T$ . As the restoring term becomes small, the width of the buoyancy-forced boundary current becomes large. As the strength of the buoyancy forcing is increased, the two imaginary components coalesce into one. Even

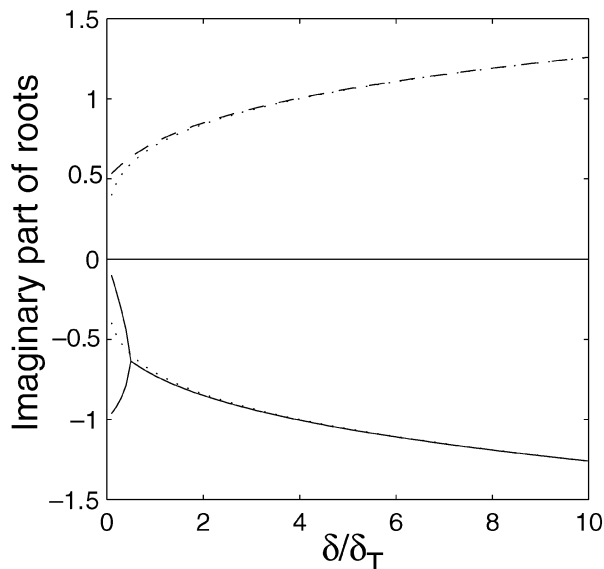


FIG. 2. Imaginary components that control the offshore exponential decay. The solid lines are the negative imaginary components for the eastern boundary layer and the dashed line is the positive imaginary component for the western boundary layer solution from (7). The dotted lines are the approximate strong forcing values given by (8) and (9).

as the damping length scale becomes small ( $\delta/\delta_T \gg 1$ ), there is only a single offshore decay scale primarily governed by the viscous length scale  $\delta$  [the imaginary parts of  $k_1$  and  $k_2$  are  $O(1)$ ]. The dashed line indicates the imaginary components of the roots  $k_3$  and  $k_4$  appropriate for the western boundary layer solution. The western boundary layer always remains  $O(\delta)$  in width, with slightly wider boundary layers as the buoyancy-forcing becomes weak.

In addition to the full solution to (7), one can obtain a useful approximate solution for the roots in the strong buoyancy forcing limit,  $\delta/\delta_T \gg 1$ . In this case, the second term of (7), which arises because of the  $\beta$  term in the vorticity equation, is negligible and the roots can be solved for directly:

$$k_{1,2} = \frac{\sqrt{2}}{2}(\pm 1 - i)\left(\frac{\delta}{\delta_T}\right)^{1/4} (1 + \beta y)^{1/2} \quad \text{and} \quad (8)$$

$$k_{3,4} = \frac{\sqrt{2}}{2}(\pm 1 + i)\left(\frac{\delta}{\delta_T}\right)^{1/4} (1 + \beta y)^{1/2}. \quad (9)$$

These approximate solutions with  $y = 0$  are shown in Fig. 2 as the dotted lines. For  $\delta/\delta_T > 1$ , the comparison is generally quite close to the solution of the full equation. This approximate form will be used later in obtaining closed form solutions for the boundary layer structure and circulation around the island.

The solution procedure is outlined for the eastern boundary layer. A similar approach has been taken for the western boundary layer using roots  $k_3$  and  $k_4$  instead of  $k_1$  and  $k_2$ . The perturbation pressure is written as the

sum of the two eastern boundary layer solutions, each with an amplitude that varies in  $y$ :

$$P(x, y) = A(y)e^{ik_1x} + B(y)e^{ik_2x}. \quad (10)$$

The relationship between the coefficients  $A$  and  $B$  is provided by the lateral boundary condition on the meridional velocity. For no-slip boundaries,  $v = P_x = 0$  at  $x = 0$  so that

$$B = -\frac{k_1}{k_2}A. \quad (11)$$

The meridional momentum equation and the no-normal flow boundary condition at  $x = 0$  are used to solve for the meridional dependence of the perturbation pressure  $A$ . The nondimensional form of the steady, linear meridional momentum equation is written as

$$(1 + \beta y)u + p_y = \beta \frac{P_{xxx}}{(1 + \beta y)}. \quad (12)$$

The zonal velocity may be defined as the sum of the geostrophic flow that balances the large-scale meridional pressure gradient,  $U = -P_y/(1 + \beta y)$ , and  $u'$  due to the presence of the boundary so that  $u = U + u'$ .

The nondimensional equation for the perturbation pressure  $P$  is then written as

$$(1 + \beta y)u' + P_y = \beta \frac{P_{xxx}}{(1 + \beta y)}. \quad (13)$$

At the boundary, the no-normal-flow condition requires that  $u' = -U$ , so

$$P_y = \frac{\beta P_{xxx}}{1 + \beta y} + (1 + \beta y)U. \quad (14)$$

Substitution of (10) and (11) into (14) results in a single equation for the function  $A$ :

$$A_y = \left(\frac{C_1}{1 + \beta y} + C_3\right)A + (1 + \beta y)C_2. \quad (15)$$

This is similar to the equation derived by McCreary (1981) and used by McCreary et al. (1986) to model the Leeuwin Current, although they neglected a term analogous to  $C_3A$  on the right-hand side.

The coefficients are

$$C_1 = -i\beta k_1 k_2 (k_1 + k_2), \quad C_2 = \frac{k_2 U}{k_2 - k_1}, \quad \text{and}$$

$$C_3 = \frac{k_2}{k_2 - k_1} \frac{\partial k_1/k_2}{\partial y}. \quad (16)$$

The coefficient  $C_3$  depends on the meridional gradient of the ratio  $k_1/k_2$ . In the strong buoyancy-forcing limit, (8) indicates that  $k_1/k_2$  is independent of  $y$  so that this term can be neglected. For weak buoyancy forcing and small islands, the terms proportional to  $C_1$  and  $C_3$  are small in comparison with the  $C_2$  term ( $A$  increases linearly with latitude). The only circumstance for which

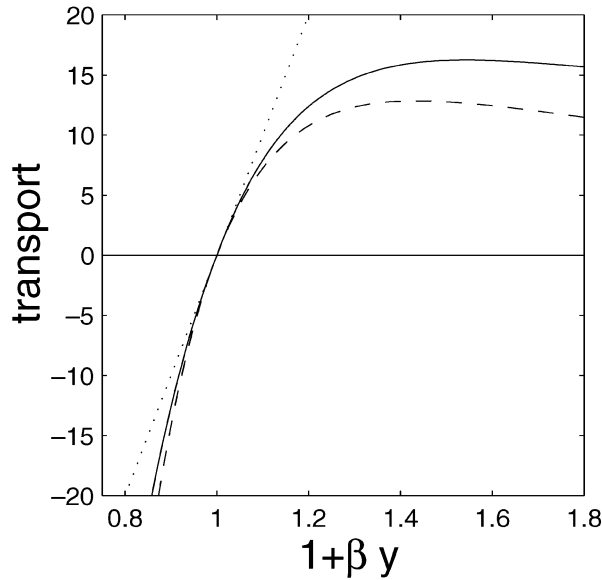


FIG. 3. Transport in the eastern boundary current as a function of Coriolis parameter  $f = 1 + \beta y$  for  $\delta/\delta_r = 5$ . The solid line is the full numerical solution to (7) and (15). The dashed line is the approximate closed-form solution (18). The dotted line is the total transport approaching the boundary from the west between the stagnation point and latitude  $y$ . Poleward of the stagnation point, the boundary current transports less than this amount, which indicates downwelling (and cooling) near the boundary. Equatorward of the stagnation point, the boundary current transports more water toward the equator than approaches from the interior, indicating upwelling (and heating) near the boundary.

the  $C_3$  term is important is for weak buoyancy forcing and large islands. In this case, the meridional variation in  $k_1/k_2$  becomes large near the equatorward end of the island. The neglect of this term by McCreary et al. (1986) was valid for the problems that they studied because the buoyancy forcing in their cases was always strong and their boundary currents remained far from the equator.

The amplitude  $A$  can be determined by integrating (15) numerically, noting that the coefficients  $C_1$ ,  $C_2$ , and  $C_3$  are functions of  $y$ . An example of the meridional transport in the eastern boundary current as a function of latitude is shown in Fig. 3 for the case  $\delta/\delta_r = 5$  and  $U = 1$ . The solid line is the direct numerical integration of (15) with the roots  $k_1$  and  $k_2$  solved numerically from (7). There exists a stagnation point at  $y = 0$ , where the perturbation pressure vanishes. The transport is poleward for  $y > 0$  and equatorward for  $y < 0$ . The boundary current approaches its maximum poleward transport near  $y = -C_1^{-1}$  while it grows exponentially toward the equator.

The basic structure of the amplitude  $A$ , and hence the transport, can be readily anticipated from (15) by considering the limit in which the Rossby wave speed is independent of latitude [set  $y = 0$  in (15) and (7)] and neglecting the  $C_3$  term. For this case, the function  $A$  grows exponentially with meridional scale  $C_1^{-1}$  as

$$A = -\frac{C_2}{C_1}(1 - e^{C_1 y}). \tag{17}$$

The amplitude equilibrates for  $y > 0$  at a value of  $-C_2/C_1$ . If it is further assumed that  $\delta/\delta_r \gg 1$ , so that the approximate roots (8) and (9) can be used, the transport  $T$  can be written as

$$T = U(1 - e^{C_1 y})/[\sqrt{2}\beta f(\delta/\delta_r)^{3/4}]. \tag{18}$$

This estimate compares reasonably well with the full solution for moderate values of  $y$ , as indicated in Fig. 3 by the dashed line. The amplitude is underestimated for large  $y$  because, if one takes into account the  $y$  dependence in (15) and for the roots  $k_{1,2}$ , the transport decreases only as  $f^{-1/2}$  for  $y \gg -C_1$  (large islands). The transport estimate (18) will be used in section 3 for estimating the circulation around an island.

The dotted line in Fig. 3 indicates the magnitude of the eastward transport toward the boundary between the stagnation point and latitude  $y$ . An eastern boundary current transport of this amount corresponds to all of the eastward transport turning and flowing parallel to the boundary in the eastern boundary current. For planetary-scale eastward flows ( $\beta y > 0.1$ ), the poleward transport in the eastern boundary current is always much less than the total transport toward the boundary. This implies that there is significant downwelling near the eastern boundary in the poleward boundary current, as has been inferred to occur along the southwest coast of Australia by Godfrey and Ridgway (1985). For  $y < 0$ , the equatorward transport in the eastern boundary current is larger than this eastward transport, indicating upwelling and heating equatorward of the stagnation point.

One finds a similar behavior for the buoyancy-forced western boundary currents except that the boundary current transport is toward the stagnation point instead of away from the stagnation point. The boundary current transport grows exponentially toward the pole and, for  $\delta \gg \delta_r$ , equilibrates to (18) toward the equator. The same expression applies to both the western and eastern boundary currents because, in the limit  $\delta \gg \delta_r$ , the beta term in the vorticity equation is negligible. Although the pressure anomaly is the same at each tip of the island, the transport at the equatorward end in the western boundary current will always be larger than the transport at the poleward end in the eastern boundary current because  $f_e < f_p$ .

This approach differs from the buoyancy-forced eastern boundary current model discussed by Spall (2000) in several significant ways. Most important, the vertical motions were specified in Spall (2000), while here they arise as a result of anomalous upper-ocean layer thickness and air-sea heat flux. As a result, the spatial scale, magnitude, and even sign of the upwelling and downwelling regions are determined as part of the solution. This results in different phenomena, such as stagnation points on the boundary and strong poleward and equatorward

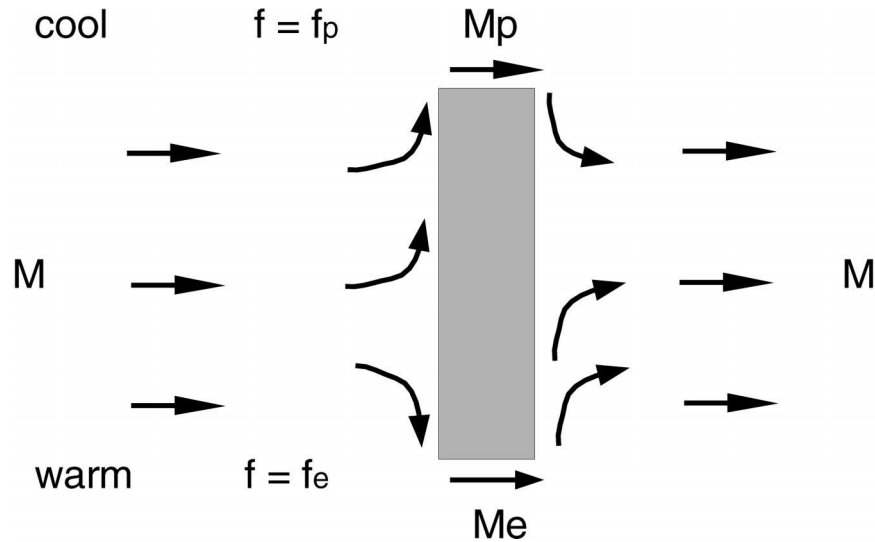


FIG. 4. Schematic of the large-scale circulation for an island embedded in an upper-ocean eastward geostrophic flow. The eastward upper-ocean transport is  $M$ , the transport around the poleward tip of the island is  $M_p$ , and the transport around the equatorward tip of the island is  $M_e$ .

torward eastern boundary currents. However, both models indicate that dissipation can be important along eastern boundaries when buoyancy forcing is active.

### 3. Circulation around an island

The stagnation point, or  $f_0$ , the Coriolis parameter at  $y = 0$ , is a free parameter of the analytic model derived in the previous section. This parameter was not specified in the eastern boundary current models of McCreary et al. (1986) or Weaver and Middleton (1990), but was only assumed to lie equatorward of the forcing region. However, the boundary current structure and circulation around the island clearly depend on the value of the stagnation point. A circulation integral may be used to determine where the stagnation point is located.

A schematic of the buoyancy-forced circulation with an island is shown in Fig. 4. In general, the eastward transport  $M$  impinges on the west coast of the island and splits into equatorward and poleward eastern boundary currents (as in Fig. 3). Stagnation points are found on both the western and eastern sides of the island. The stagnation point on the western (eastern) side of the island will generally be found equatorward (poleward) of the midlatitude of the island.

Geostrophy requires that warm water lie to the right of the upper-ocean flow in the Northern Hemisphere. Any equatorward eastern boundary current transport ( $M_e$ ) will flow cyclonically around the equatorward tip of the island and any poleward eastern boundary current transport ( $M_p$ ) will flow anticyclonically around the poleward tip of the island. The lack of zonal jets west of the island tips in the basin interior is an important difference between the buoyancy-forced circulation and

the wind-driven circulation around an island discussed by Godfrey (1989). The zonal flow in the eastern basin draws its transport from the western boundary layer along the eastern side of the island. Some of this transport upwells in the western boundary layer and some originates from the western side of the island and is carried to the east in the narrow boundary currents that pass around the tips of the island.

The regions equatorward of the stagnation points are anomalously cold, resulting in heating by the atmosphere and upwelling. The regions poleward of the stagnation points are anomalously warm and result in cooling by the atmosphere and downwelling. This cooling and downwelling in the poleward boundary current along the western side of the island is analogous to what is found in the Leeuwin Current, where there is strong heat loss to the atmosphere and downwelling has been inferred from hydrographic data (Godfrey and Ridgway 1985).

The steady solution is determined by imposing a circulation integral around the island. As discussed by Pedlosky et al. (1997) and Spall (2000), in the absence of wind forcing the integral of dissipation around an island must vanish. This circulation integral, together with the analytic solution for the eastern and western boundary layers, provides the necessary constraints to determine the stagnation points, the transports in the boundary currents, and the circulation around the island. For either linear dynamics or no-slip boundary conditions, dissipation must be balanced by a change in pressure along the boundary, and so one may discuss the dissipation integral in terms of the pressure change along the boundary. The solution has been obtained by starting with the western stagnation point at the southern tip of the island

and integrating (15), together with (10), (11) (and their western boundary current counterparts), and (7), around the island. It is assumed that the pressure is continuous around the poleward and equatorward tips of the island. If the pressure at the end of this integration around the island is not zero (so that it matches the zero pressure at the starting point of the integration), the location of the stagnation point is moved poleward, and the circulation integral is calculated again. This process is repeated until the pressure is continuous around the island. The circulation has been found as a function of the nondimensional change in Coriolis parameter over the meridional extent of the island ( $\beta L_I$ ) and the ratio of the viscous boundary layer width to the thermal boundary layer width ( $\delta/\delta_T$ ).

The strength of the circulation around the equatorward and poleward tips of the island normalized by the total eastward flow ( $M_e/M$ ,  $M_p/M$ ) is shown in Figs. 5a and 5b. For all parameter values explored here, a significant fraction of the eastward transport in the western basin circulates around the tips of the island into the eastern basin. For small islands subject to weak buoyancy forcing (lower-left region of the figures), approximately one-half of the eastward transport passes around each end of the island and into the eastern basin. This is expected because, in this limit, the equations are symmetric in latitude. The effects of variable Rossby wave phase speed with latitude are negligible for small islands, and the pressure variation along the boundary is nearly linear with latitude for weak forcing. This transport is not very sensitive to increases in the buoyancy forcing as long as the island remains sufficiently small. However, for weak buoyancy forcing and large islands, the equatorward transport increases and the poleward transport decreases. This is largely because the geostrophic transport depends on  $P/f$  and, for weak forcing, the pressure anomaly at each end of the island is nearly the same magnitude (and of opposite sign) but  $f_e < f_p$ . As the buoyancy forcing increases and the island becomes large, the fraction of the eastward transport that circulates around the island into the eastern basin decreases. This is because the pressure (or temperature) change from the equatorward to the poleward tip of the island is increased. More of the interior upper-layer thickness contours intersect the boundary on both the eastern and western sides of the island (see, e.g., Fig. 1). The equatorward transport remains  $f_p/f_e$  greater than the poleward transport because of the lower value of the Coriolis parameter at the equatorward end of the island.

For sufficiently strong buoyancy forcing, approximate closed-form solutions can be obtained by recognizing that the magnitude of the pressure anomaly at the poleward end of the island must match that at the equatorward end of the island. This condition can be used, together with the approximate closed-form solution (18), to estimate the transport around the poleward and

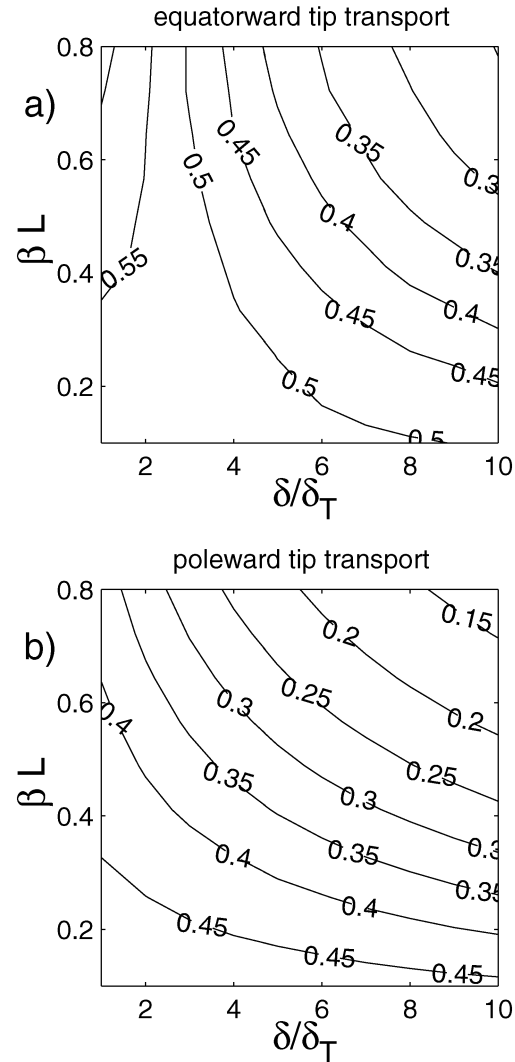


FIG. 5. Analytic solution for the island circulation as a function of island extent  $\beta L_I$  and strength of thermal forcing  $\delta/\delta_T$ : (a) transport around the equatorward tip of the island normalized by the eastward transport,  $M_e/M$ ; (b) transport around the poleward tip of the island normalized by the eastward transport,  $M_p/M$ .

equatorward tips of the island, relative to the eastward transport  $M$ , as

$$\frac{M_e}{M} = \frac{\tanh(\alpha/2)}{f_e \alpha} \quad \text{and} \quad \frac{M_p}{M} = \frac{\tanh(\alpha/2)}{f_p \alpha}, \quad (19)$$

where  $\alpha = \sqrt{2}\beta L_I (\delta/\delta_T)^{3/4}$ .

These approximate closed-form solutions compare well to the full numerical solution over most of the parameter range (Fig. 6). There is a small difference when the buoyancy forcing is very weak, as expected. These solutions show that the main difference between the transport around the poleward and equatorward tips of the island is due to the change in the Coriolis parameter.

The decrease in transport around both ends of the

island with increasing  $\beta L_i$  and  $\delta/\delta_T$  implies that there must be an increase in downwelling along the western side of the island and in upwelling on the eastern side. The net downwelling in the western basin is shown in Fig. 7. For weak buoyancy forcing or small islands, there is very little net downwelling. There is downwelling poleward of the stagnation point and upwelling equatorward of the stagnation point, but they are nearly equal in magnitude so that the net vertical motion west of the island is small. As the island increases in size, or the buoyancy forcing increases, the stagnation point shifts equatorward and the net vertical motion is dominated by the downwelling.

#### 4. Numerical examples

The analytic model developed in the previous section is now compared with results using the Miami Isopycnal Coordinate Ocean Model (MICOM), which solves the primitive equations of motion using isopycnal coordinates in the vertical. The version of the model used here is a simplified version of the full model described by Bleck et al. (1992). The model is configured with two isopycnal layers, and temperature and salinity are constant within each layer. There is no wind stress or surface buoyancy flux so that there is no active mixed layer. Subgrid-scale mixing is limited to along-isopycnal Laplacian viscosity with no-slip lateral boundary conditions. The model is forced by restoring the interface between the two moving layers to a uniform meridional gradient with timescale  $\gamma$ .

There are three length scales specified for the model: the inertial boundary layer thickness  $\delta_i = (U/\beta^*)^{1/2}$ ; the viscous boundary layer thickness  $\delta = (A/\beta^*)^{1/3}$ ; and the thermal damping length scale  $\delta_T = \beta^* L_a^2 \gamma$ , where  $L_a = \sqrt{g'H/2/f}$  is the internal deformation radius. The strength of the eastward upper layer flow  $U$  is inferred from  $\delta_i$ . The strength of the lateral viscosity is calculated from the Munk layer thickness  $\delta$ . One additional non-dimensional parameter needs to be defined, the ratio of the advective speed to the baroclinic Rossby wave phase speed,  $F = U/\beta^* L_a^2$ . The results are not sensitive to this parameter because the purely baroclinic flow to the west of the island does not influence the propagation speed of the baroclinic waves that set up the steady solution (e.g., Killworth et al. 1997). However, consideration of higher vertical modes can result in some trapping due to this nonlinear effect (McCreary et al. 1992). The reduced gravity between the two layers is calculated from  $F$  as  $g' = (\rho_2 - \rho_1)g/\rho_0 = 2\delta_i^2 f_0^2 / FH$ . The time-scale of the interface restoring term is calculated from the definition of  $\delta_T$ , which will be varied.

The model domain is 1500 km in zonal extent and 3000 km in meridional extent. The grid spacing is uniform at 25 km, and the central Coriolis parameter  $f_0 = 6 \times 10^{-5} \text{ s}^{-1}$ , the meridional gradient of the Coriolis parameter  $\beta^* = 2 \times 10^{-11} \text{ m}^{-1} \text{ s}^{-1}$ , and the resting layer thicknesses  $H = 200 \text{ m}$  are specified. The inertial

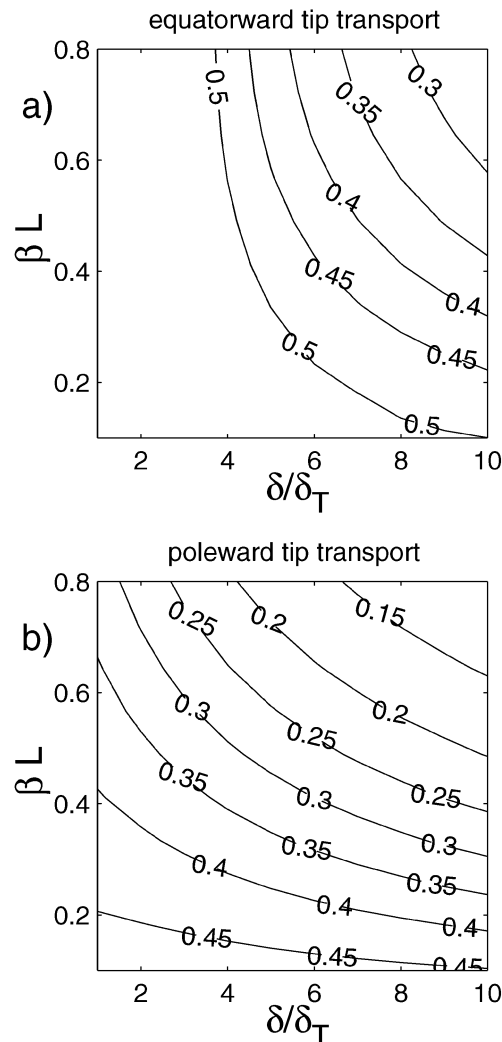


FIG. 6. Closed-form analytic solution (19) as a function of island extent  $\beta L_i$  and strength of thermal forcing  $\delta/\delta_T$ : (a) transport around the equatorward tip of the island normalized by the eastward transport,  $M_e/M$ ; (b) transport around the poleward tip of the island normalized by the eastward transport,  $M_p/M$ .

boundary layer width  $\delta_i = 40 \text{ km}$  ( $U = 3.2 \text{ cm s}^{-1}$ ), and the frictional boundary layer width  $\delta = 60 \text{ km}$ . The ratio of the advective speed to the Rossby wave phase speed  $F = 1$ .

As an example, a rectangular island that extends 1950 km in the meridional direction ( $\beta L_i = 0.65$ ) and 100 km in the zonal direction located in the center of the domain is first considered. The model is initialized at rest and run for a period of 20 years, at which time the fields are essentially steady.

The upper-layer circulation with a buoyancy-forcing strength of  $\delta/\delta_T = 4$  is shown in Fig. 8a. The flow in the interior to the west of the island is uniform and toward the east. As this eastward flow approaches the island it splits into poleward and equatorward eastern boundary currents. The maximum speed in the poleward



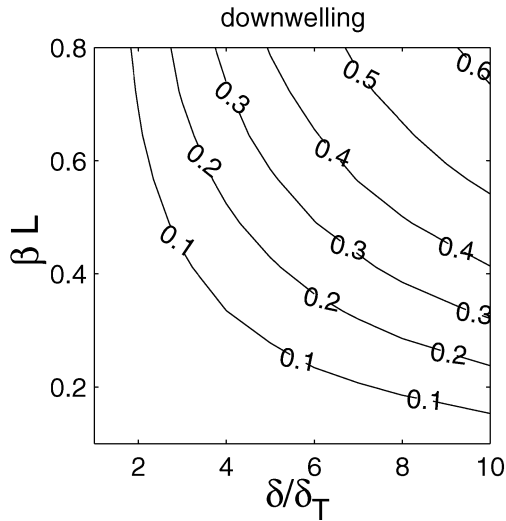


FIG. 7. Net downwelling in the western basin (scaled by the eastward transport  $M$ ) as a function of island extent  $\beta L_i$  and strength of thermal forcing  $\delta/\delta_T$  from the analytic solution.

boundary current is now an order of magnitude larger than found in the interior. The velocity and transport of the poleward boundary current have essentially equilibrated at the poleward end of the island, but the equatorward boundary current is still increasing in strength toward the equator. The transport and velocity structure of the boundary currents are in good agreement with the analytic solution in the previous section (not shown). The stagnation point along the eastern side of the island lies poleward of the midlatitude of the island. Significant transports from the western basin into the eastern basin are found around both ends of the island.

The thickness of the upper layer is shown in Fig. 8b. The thickness in the interior of each basin is essentially the same as the restoring thickness  $\mathcal{H}$ . (Note that similar boundary currents are found on the eastern and western boundaries of the basin but they have no influence on the circulation around the island and will not be discussed.) The poleward boundary current along the western side of the island is thick (warm) while the equatorward boundary current is thin (cold) in comparison with the interior thickness  $\mathcal{H}$  at the same latitude. The layer thickness, and thus pressure, vary along both the

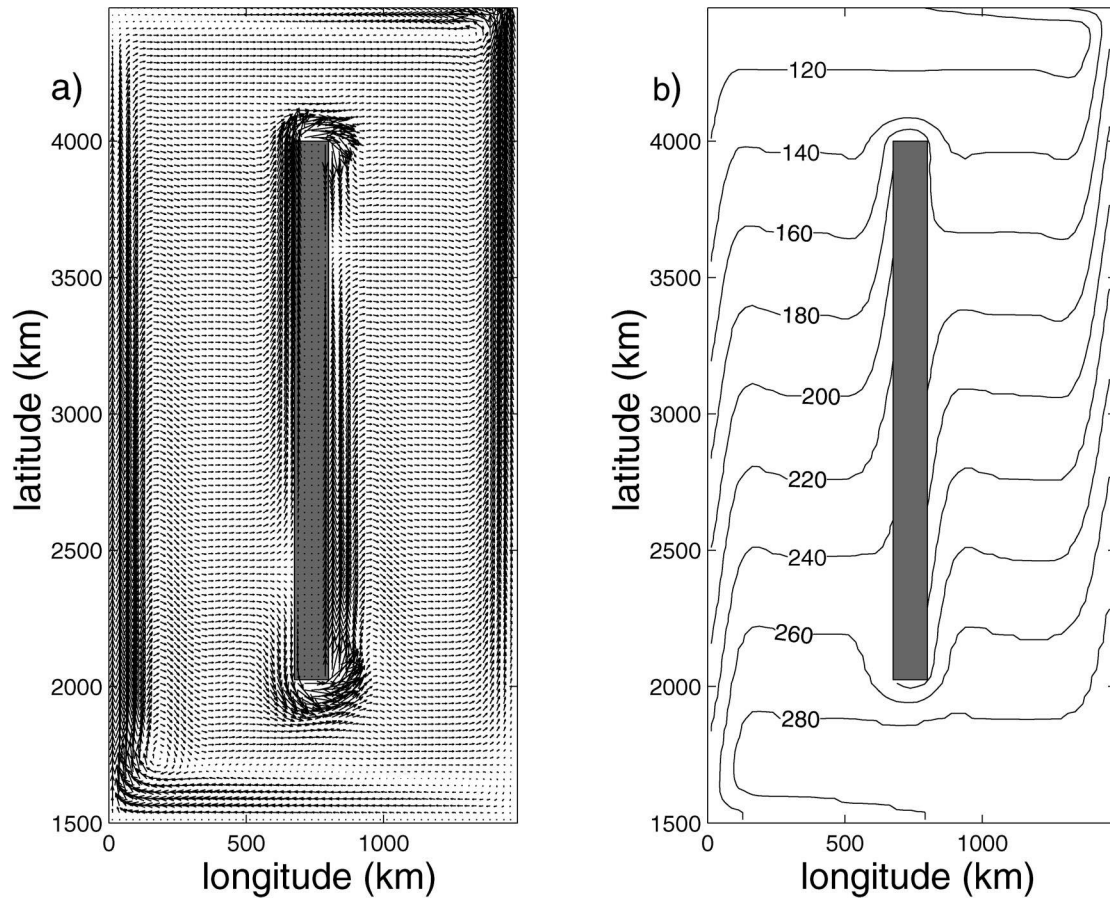


FIG. 8. Steady upper layer (a) velocity and (b) layer thickness (m) from a two-layer primitive equation numerical calculation. The nondimensional island dimension  $\beta L_i = 0.65$ , and the thermal forcing  $\delta/\delta_T = 4$ . Approximately 40% (22%) of the eastward transport circulates around the equatorward (poleward) tip of the island, in reasonable agreement with the theory.

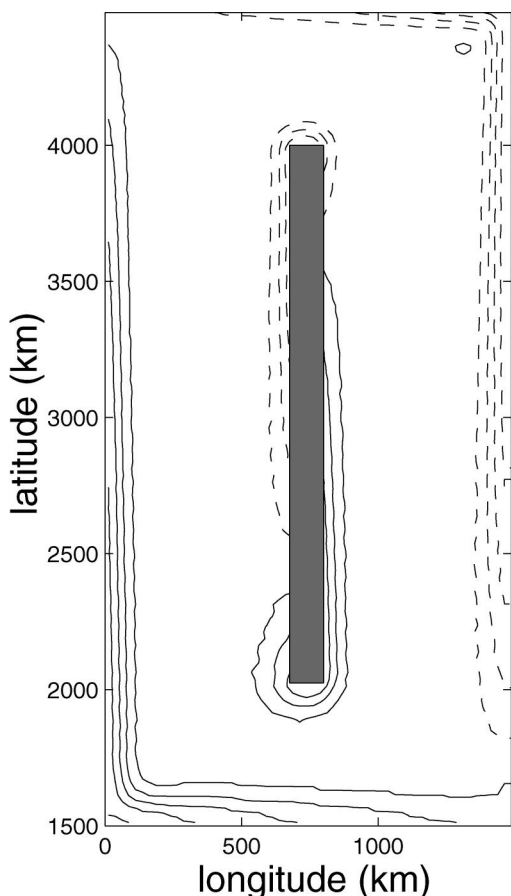


FIG. 9. Vertical velocity at the layer interface (contour interval  $1 \text{ m day}^{-1}$ , dashed negative) from the calculation shown in Fig. 8. There is downwelling along both sides of the island poleward of the stagnation points and upwelling equatorward of the stagnation points. For such a large island, the net vertical motion on the western (eastern) side of the island is dominated by downwelling (upwelling).

western and eastern sides of the island as a result of the buoyancy forcing.

The vertical velocity is shown in Fig. 9. The vertical motion is concentrated within the boundary layers described by the analytic model. There is downwelling where the boundary current is anomalously warm and upwelling where the boundary current is anomalously cold. Most of the western side of the island is dominated by downwelling of  $O(3 \text{ m day}^{-1})$ . For this calculation, approximately 40% of the eastward transport to the west of the island downwells in the western basin. Note that some of the water that flows into the eastern basin around the equatorward tip of the island originates in the interior of the western basin and some has been upwelled along the western side of the island. The water that feeds the interior eastward flow in the eastern basin originates both from the western basin and from upwelling within the western boundary current of the eastern basin.

A series of numerical calculations have been carried

out in which the buoyancy forcing is varied as  $\delta/\delta_T = 1, 2, 4, 6, 8, 10$  and the size of the island is varied such that  $\beta L_I = 0.15, 0.25, 0.35, 0.45, 0.55, 0.65, 0.75$ . The strength of the transport around the equatorward and poleward tips of the island diagnosed from these 42 calculations is shown in Fig. 10. The amplitude and general pattern are in close agreement with the theory in Fig. 5. There is also a net downwelling in the western basin in the model, as shown in Fig. 11. The model produces slightly more downwelling than is predicted by the theory, but the general parameter dependence and amplitude are in agreement with the theory in section 2.

## 5. Discussion

Although the approach taken here uses a circulation integral to determine the circulation around an island, the results differ from the original barotropic, wind-driven island rule proposed by Godfrey (1989) in several important ways. The attractiveness of the wind-driven island rule is that one can estimate the circulation around the island without specific knowledge of the (not well understood) mixing processes in the ocean. This results from careful choice of the integration path and the inability of wind-forcing to result in any significant dissipation on eastern boundaries (the western side of the island). However, no analogous path is available to estimate the buoyancy-forced circulation around an island. The circulation anomalies introduced by the island are restricted to within relatively narrow boundary layers encircling the island. Thus, the circulation far from the island is not influenced by the presence of the island. For example, there are no zonal jets extending westward from the tips of the island, as for the wind-only cases. In addition, specific parameterizations of the mixing of momentum and density are required to provide solutions; thus the simple elegance of the original island rule is lost. However, useful closed-form solutions are available in the strong buoyancy-forcing limit (19). This theory also demonstrates that, over a wide range of physical parameters, a large fraction of the eastward upper-ocean geostrophic flow will circulate around the island from the western basin into the eastern basin, suggesting the baroclinic circulation may provide an important perturbation to the wind-driven circulation around large islands and alter the exchange between adjacent basins.

From a practical point of view, the primary drawback of the theory is that one needs to estimate the strength of the mixing for both momentum and density. Order-of-magnitude estimates can, however, be made. If one takes the width of the Leeuwin Current as representative of the viscous boundary layer width, then  $\delta \approx 100\text{--}150 \text{ km}$ . Godfrey and Weaver (1991) take the sensitivity of the surface heat flux to anomalous sea surface temperature as  $\lambda = 35 \text{ W m}^{-2} \text{ }^\circ\text{C}^{-1}$ . This gives a relaxation timescale over a mixed layer depth of  $H = 100 \text{ m}$  to

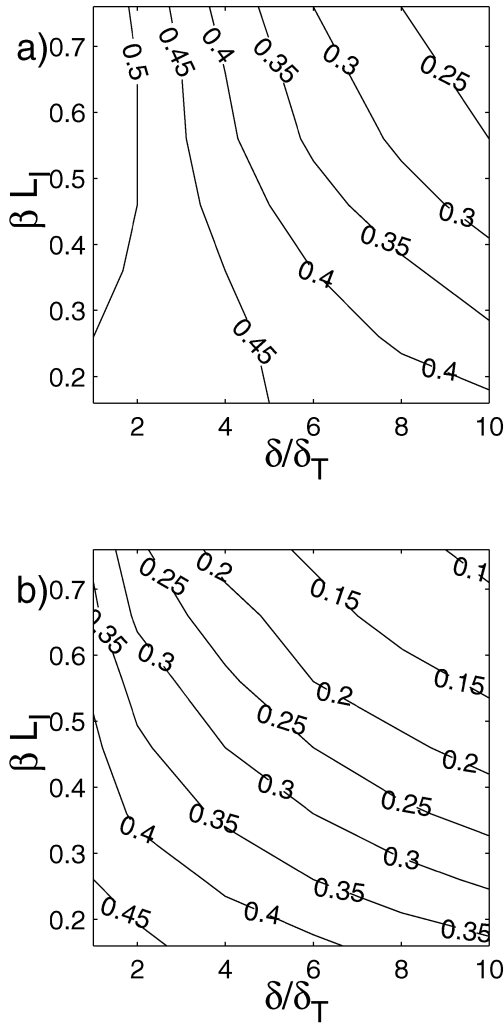


FIG. 10. The circulation around the island as a function of island extent  $\beta L_l$  and strength of thermal forcing  $\delta/\delta_T$  diagnosed from a series of primitive equation model calculations: (a) transport around the equatorward tip of the island normalized by the eastward transport,  $M_e/M$ ; (b) transport around the poleward tip of the island normalized by the eastward transport,  $M_p/M$ .

be  $\gamma = \rho_0 C_p H / \lambda = 10^7$  s. Godfrey and Weaver (1991) and McCreary et al. (1986) find that it is the second-vertical-mode Rossby wave that sets up the Leeuwin Current (LC) because of the small vertical scale of the LC in comparison with the depth of the main thermocline in the Indian Ocean. Taking a typical Kelvin wave speed along the west coast of Australia as  $\sqrt{g'H} = 2$  m s<sup>-1</sup>, the phase speed of the second-vertical-mode Rossby wave is  $c = 0.25\beta g'H/f_0^2 \approx 0.5$  cm s<sup>-1</sup>. The thermal boundary layer width is then  $\delta_T = c\gamma \approx 50$  km. While the uncertainty in these numbers is large, these estimates suggest that  $\delta/\delta_T = O(2-3)$  along the west coast of Australia.

The results in Figs. 5 and 10 suggest that, for  $\delta/\delta_T = O(2-3)$ , the circulation is not overly sensitive to the meridional scale of the island. Nonetheless, it is useful

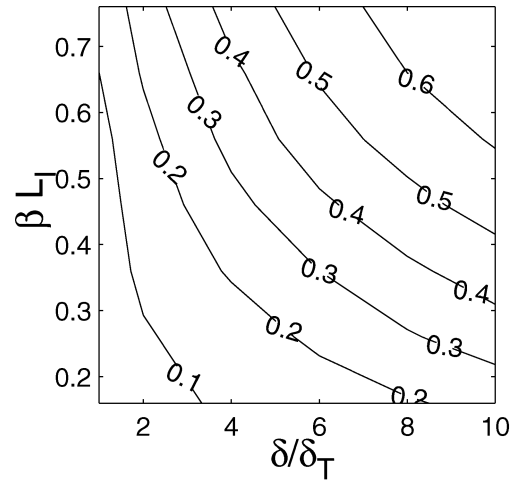


FIG. 11. The net downwelling, scaled by the eastward transport, west of the island as a function of island extent  $\beta L_l$  and strength of thermal forcing  $\delta/\delta_T$  diagnosed from a series of primitive equation model calculations.

to calculate  $\beta L_l$  for several islands of interest. The meridional extent of the eastward flow to the west of Australia is  $L_l \approx 2300$  km, while  $\beta^* = 2 \times 10^{-11}$  m<sup>-1</sup> s<sup>-1</sup> and  $|f_0| = 0.6 \times 10^{-4}$  s<sup>-1</sup>, so that  $\beta^* L_l / f_0 \approx 0.8$ . The relative change in the Coriolis parameter over the latitude range of the island may also be calculated for New Zealand ( $\beta^* L_l / f_0 \approx 0.3$ ) and Madagascar ( $\beta^* L_l / f_0 \approx 0.56$ ).

The eastward geostrophic flow at the surface in the eastern Indian Ocean can be estimated from Fig. 1 to be  $u = -g\eta_y/f_0 \approx 0.04$  m s<sup>-1</sup>, where  $\eta_y = 0.5$  m/2300 km =  $2.17 \times 10^{-7}$  is the meridional gradient in the sea surface steric height. The eastward transport is then calculated as  $M = uHL_l/2 \approx 8$  Sv, where  $H = 200$  m is the thickness of the upper layer,  $L_l = 2300$  km is the meridional extent of the region of eastward flow, and it has been assumed that the zonal velocity decreases linearly to zero at depth  $H$ . The poleward transport in the Leeuwin Current at the southern tip of Australia can also be estimated from the dynamic height to be approximately 2 Sv (Sv  $\equiv 10^6$  m<sup>3</sup> s<sup>-1</sup>).

The theory produces a similar transport in the poleward eastern boundary current of  $M_p = 0.27M = 2.2$  Sv for  $\delta/\delta_T = 3$  and  $\beta L_l = 0.8$ . The theory predicts a net downwelling along the west coast of Australia of  $0.25M = 2$  Sv and an upper-ocean circulation from the Indian Ocean into the Pacific Ocean through the Indonesian Throughflow of strength  $M_e = 0.48M = 3.8$  Sv.

Some caution must be used in applying the theory to the circulation around the equatorward end of Australia because of the complexity of the islands and straits that make up the throughflow, proximity to the equator, and because of the idealized buoyancy forcing used for the theory. However, model calculations indicate that many of the characteristics previously described are also found

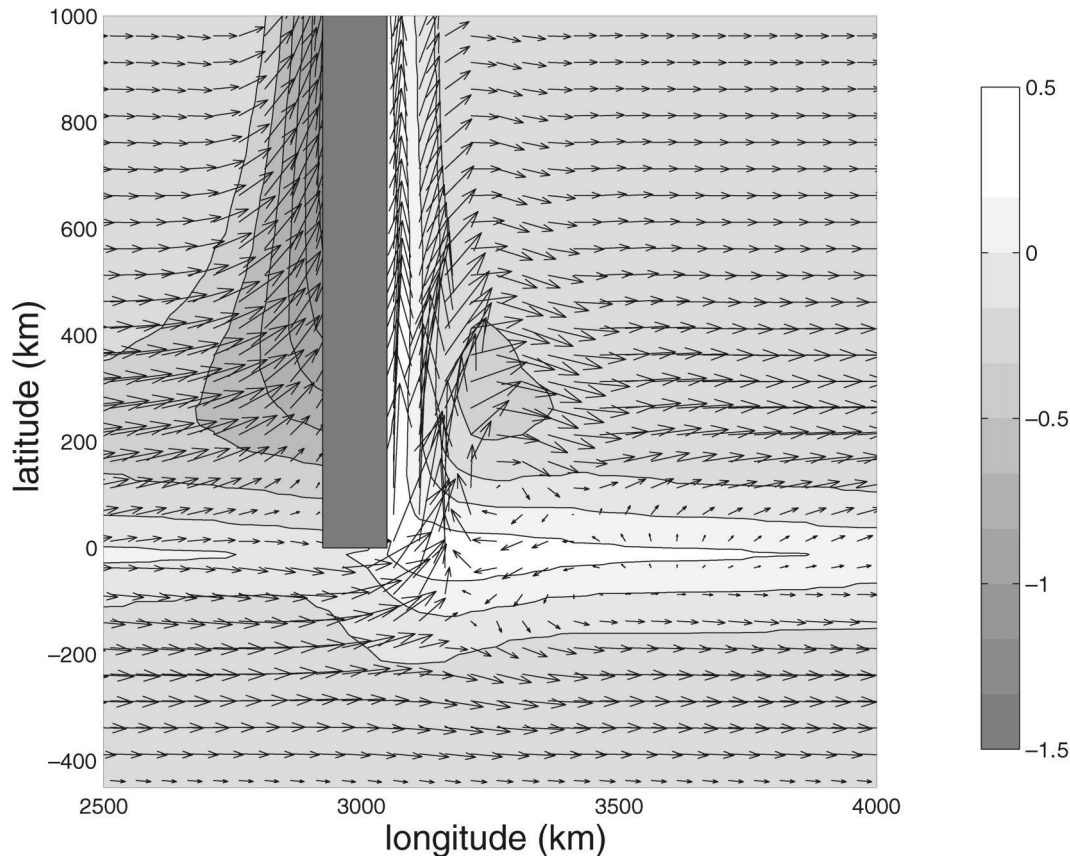


FIG. 12. Upper-layer horizontal velocity (every other point) and vertical velocity (contour interval  $0.2 \text{ m day}^{-1}$ ) at the layer interface for a case in which the southern tip of the island extends all the way to the equator,  $\beta L_I = 1.8$ , and  $\delta/\delta_T = 3$ .

for cases in which the island extends all the way to the equator. Figure 12 shows the upper-layer velocity together with the upwelling near the equatorward end of the island for a case in which the southern tip of the island lies on the equator,  $\beta L_I = 1.8$ , and  $\delta/\delta_T = 3$ . In this calculation, the zonal extent of the basin has been increased to 6000 km so that the effects of the eastern and western boundaries of the basin near the equator remain far from the island. There exist poleward boundary currents on both sides of the island with downwelling along the western boundary and upwelling along the eastern boundary. The stagnation point on the western side of the island has shifted all the way to the equatorward tip of the island so that there is downwelling all along the western side of the island. A feature not found in midlatitudes is the region of strong upwelling within approximately 200 km of the equator that is largest in a warm pool near the eastern side of the island. Thus, the transport that feeds the poleward western boundary current on the eastern side of the island originates both from the western basin and from upwelling along the equator in the eastern basin. Because the stagnation point has shifted to the equatorward tip of the island, the transport supplied to the eastern

basin from the west now comes from the opposite hemisphere. It is difficult to anticipate how the islands of Indonesia and the Philippines, and more realistic buoyancy forcing and wind forcing, will alter the source waters, but these results suggest that at least some of the eastern boundary current waters will originate in the Indonesian seas and thus might influence the baroclinic structure of the Indonesian Throughflow.

## 6. Summary

The main objective of this study is to understand the consequences of a meridional gradient in sea surface temperature on the baroclinic circulation around islands. This problem is motivated by planetary-scale islands such as Australia, New Zealand, Madagascar, Japan, and Hawaii. The general trend of decreasing sea surface temperature with increasing latitude gives rise to a geostrophically balanced eastward flow in the upper ocean. It is found that for sufficiently small islands or weak buoyancy forcing that approximately one-half of this eastward transport passes around each end of the island, where it then smoothly joins the eastward flow east of the island. However, as the island become large, such

that the meridional change in the Coriolis parameter becomes a significant fraction of the Coriolis parameter at the central latitude of the island, the exchange between the basins is reduced. A significant fraction of the eastward flow to the west of the island downwells in a narrow eastern boundary current along the west side of the island. A similar amount of water upwells within a narrow boundary current along the east coast of the island. However, even in this large-island, strong-buoyancy-forcing limit there remains an exchange between the western basin and the eastern basin through narrow boundary currents around the tips of the island. The sense of circulation is always from the western basin into the eastern basin in the upper ocean and from the eastern basin into the western basin in the deep ocean. A simple analytic closed-form solution is available in this limit.

*Acknowledgments.* Support for this work was provided by the National Science Foundation under Grant OCE-9818337 and by the Office of Naval Research under Grant N00014-01-1-0165. This work was initiated during a visit to Hobart, Australia, which was partially supported by CSIRO and the Woods Hole Oceanographic Institution. Stuart Godfrey read early versions of this manuscript in great detail and also provided many valuable comments and suggestions.

## REFERENCES

- Bleck, R., C. Rooth, D. Hu, and L. T. Smith, 1992: Salinity-driven thermocline transients in a wind- and thermohaline-forced isopycnal coordinate model of the North Atlantic. *J. Phys. Oceanogr.*, **22**, 1486–1505.
- Davey, M. K., 1983: A two-level model of a thermally forced ocean basin. *J. Phys. Oceanogr.*, **13**, 169–190.
- Ffield, A., K. Vranes, A. L. Gordon, and R. D. Susanto, 2000: Temperature variability within Makassar Strait. *Geophys. Res. Lett.*, **27**, 237–240.
- Firing, E., B. Qiu, and W. Miao, 1999: Time-dependent island rule and its application to the time-varying North Hawaiian Ridge Current. *J. Phys. Oceanogr.*, **29**, 2671–2688.
- Godfrey, J. S., 1989: A Sverdrup model of the depth-integrated flow for the World Ocean, allowing for island circulations. *Geophys. Astrophys. Fluid Dyn.*, **45**, 89–112.
- , 1996: The effect of the Indonesian Throughflow on ocean circulation and heat exchange with the atmosphere: A review. *J. Geophys. Res.*, **101**, 12 217–12 237.
- , and K. R. Ridgway, 1985: The large-scale environment of the poleward-flowing Leeuwin Current, Western Australia: Longshore steric height gradients, wind stresses, and geostrophic flow. *J. Phys. Oceanogr.*, **15**, 481–495.
- , and A. J. Weaver, 1991: Is the Leeuwin Current driven by Pacific heating and winds? *Progress in Oceanography*, Vol. 27, Pergamon, 225–272.
- , and Y. Masumoto, 1999: Diagnosing the mean strength of the Indonesian Throughflow in an ocean general circulation model. *J. Geophys. Res.*, **104**, 7889–7895.
- Gordon, A. L., 1986: Inter-ocean exchange of thermocline water. *J. Geophys. Res.*, **91**, 5037–5046.
- , R. D. Susanto, and A. Ffield, 1999: Throughflow within Makassar Strait. *Geophys. Res. Lett.*, **26**, 3325–3328.
- Kawase, M., 1987: Establishment of deep ocean circulation driven by deep-water production. *J. Phys. Oceanogr.*, **17**, 2294–2317.
- Killworth, P. D., D. B. Chelton, and R. A. de Szoeke, 1997: The speed of observed and theoretical long extratropical planetary waves. *J. Phys. Oceanogr.*, **27**, 1946–1966.
- McCreary, J. P., 1981: A linear stratified ocean model of the coastal undercurrent. *Philos. Trans. Roy. Soc. London*, **A302**, 385–413.
- , S. R. Shetye, and P. K. Kundu, 1986: Thermohaline forcing of eastern boundary currents: With application to the circulation off the west coast of Australia. *J. Mar. Res.*, **44**, 71–92.
- , Y. Fukumachi, and P. Lu, 1992: A nonlinear mechanism for maintaining coastally trapped eastern boundary currents. *J. Geophys. Res.*, **97**, 5677–5692.
- Munk, W. H., 1950: On the wind-driven ocean circulation. *J. Meteor.*, **7**, 79–93.
- Pedlosky, J., and M. A. Spall, 1999: Rossby normal modes in basins with barriers. *J. Phys. Oceanogr.*, **29**, 2332–2349.
- , L. J. Pratt, M. A. Spall, and K. R. Helfrich, 1997: Circulation around islands and ridges. *J. Mar. Res.*, **55**, 1199–1251.
- Pratt, L. J., and J. Pedlosky, 1998: Barotropic circulation around islands with friction. *J. Phys. Oceanogr.*, **28**, 2148–2162.
- Spall, M. A., 2000: Buoyancy-forced circulations around islands and ridges. *J. Mar. Res.*, **58**, 957–982.
- Thompson, R. O. R. Y., 1987: Continental-shelf-scale model of the Leeuwin Current. *J. Mar. Res.*, **45**, 813–827.
- Wajsowicz, R. C., 1993: The circulation of the depth-integrated flow around an island with application to the Indonesian Throughflow. *J. Phys. Oceanogr.*, **23**, 1470–1484.
- , 1995: The response of the Indo-Pacific Throughflow to interannual variations in the Pacific wind stress. Part I: Idealized geometry and variations. *J. Phys. Oceanogr.*, **25**, 1805–1826.
- Weaver, A. J., and J. H. Middleton, 1990: An analytic model for the Leeuwin Current off western Australia. *Cont. Shelf Res.*, **10**, 105–122.